The EMC Effect in Spin Structure Functions

A 12 GeV letter of intent to Jefferson Lab PAC 35
December 14, 2009

K. Joo and M. Ungaro
University of Connecticut, Storrs, CT 06268

W. K. Brooks[1], H. Hakobyan, and S. Kuleshov
Universidad Técnica Federico Santa María, Valparaíso, Chile

V. Dharmawardane
New Mexico State University, Las Cruces, NM 88003

A. Daniel and K. Hicks
Ohio University, Athens, OH 45701

S. Bueltmann, S. Kuhn, and L. Weinstein
Old Dominion University, Norfolk, VA 23529

G. Gilfoyle
University of Richmond, Richmond, VA 23173

A. Deur and D. Higinbotham
Thomas Jefferson National Accelerator Facility, Newport News, VA 23606

D. Crabb, D. Day, N. Kalantarians, R. Subedi, and X. Zheng
University of Virginia, Charlottesville, VA 22901

P. E. Bosted
The College of William and Mary, Williamsburg, VA 23187
and *Thomas Jefferson National Accelerator Facility, Newport News, VA 23606*

A. W. Thomas
The University of Adelaide, Adelaide SA 5005, Australia

M. Strikman
Penn State University, University Park, PA 16802

V. Guzey
Thomas Jefferson National Accelerator Facility, Newport News, VA 23606

W. Bentz
Tokai University, 1117 Kitakaname, Hiratsuka-shi, Kanagawa 259-1292, Japan

I. Cloet
The University of Washington, Seattle WA 98195

---

[1]Contact: brooksw@cern.ch

1

Abstract

We intend to perform the first measurements of the spin-dependent EMC effect utilizing CLAS12 in Hall B. We will polarize ^{7}Li, in which a highly polarized proton is embedded in a nuclear medium, using a ^{7}LiH target. The experiment measures the spin structure function $g_1^{p|^7Li}$ in a range of $2 < Q^2 < 9$ GeV^2 and $0.1 < x < 0.7$. This spin dependent EMC effect emphasizes the quark polarization degrees of freedom within a nucleus, due to the spin dependence of the coupling between the quarks and the strong field inside the nucleus.

Contents

1 Physics overview

1.1 Introduction

The question of how the properties of hadrons bound in the nuclear medium differ from the properties of free nucleons has been looked into for nearly three decades. That the structure functions of bound and free nucleons are not equal was first discovered by the European Muon Collaboration (EMC) at CERN. As part of an extensive program, they measured structure functions on hydrogen, deuterium and iron targets. The initial goal of using iron was to increase luminosity. However, when the structure functions F_2 of the iron and deuterium were compared, they discovered that the 'per nucleon' structure function in iron differs significantly from that of deuterium. This nuclear dependence, known since as the EMC effect, has stimulated experimental and theoretical interest over the last two decades.
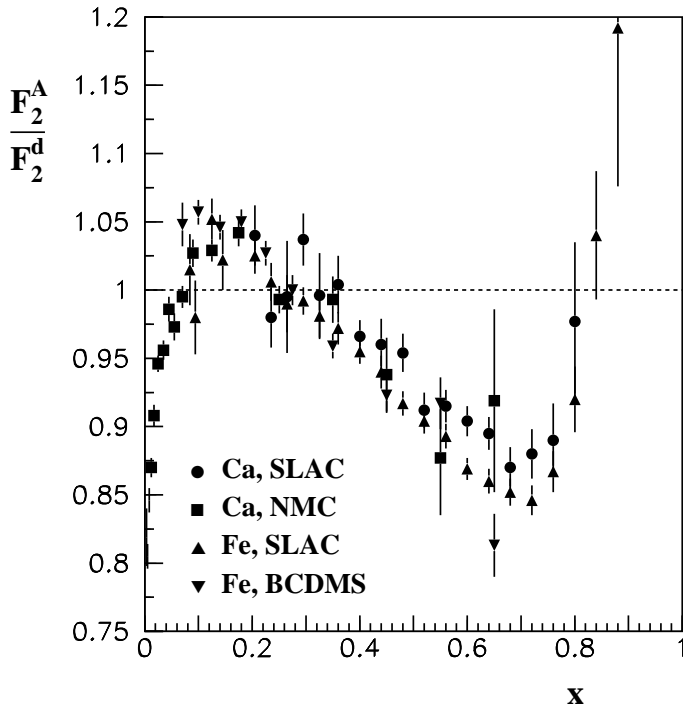

Figure 1: Experimental data for the EMC effect in the unpolarized structure function F_2 for ^{40}Ca and ^{56}Fe taken at NMC, SLAC and BCDMS.

In recent years many experiments dedicated to study the nuclear effects in unpolarized inelastic scattering have been carried out at CERN, SLAC, FNAL and JLab. Fig. 1 shows a compilation of data for the observed ratio of the structure functions 'per nucleon' for several larger nuclei and deuterium. Several distinct regions with characteristic nuclear effects are clearly identifiable from this figure: in the low x region, $(x < 0.1)$, the

nuclear structure function is reduced compared to the free nucleon structure function and around $x \approx 0.1$ the ratio rises to cross unity. In the region $0.2 < x < 0.8$ the ratio is smaller than the free nucleon structure function. This region is considered as the "EMC effect" region. In this region the ratio falls to a minimum around $x \approx 0.65$ and then rises steeply. In the very large x region the ratio rises above unity. These observations strongly suggest that the quark distributions in bound nucleons are different from those in free nucleons. Several theoretical models have attempted to explain the overall behavior seen in these ratios of unpolarized nuclear and free nucleon structure functions. However they reproduce only part of the observed behavior. The observations seen for $x < 0.1$ are explained by the shadowing phenomenon while the observed enhancement for $x > 0.8$ is associated with the Fermi motion. Several approaches have been used to explain the observed nuclear dependence in the EMC effect region. Some models have attempted to describe the EMC effect using conventional nuclear physics employing nucleonic and pionic degrees of freedom. Another category of models has assumed the existence of exotic states such as multiquark clusters in nuclei. A different approach used by rescaling models postulates that the scale Q^2 or the variable x for a bound nucleon is different from that of a free nucleon. Despite a tremendous effort, there exists at present still no unambiguously accepted explanation of the EMC effect.

The modification of hadron properties in the nuclear environment is of fundamental importance in understanding the implications of QCD for nuclear physics. In QCD, the properties of hadrons are strongly influenced by the induced sea of quark-antiquark pairs and the gluons produced in the confining interactions. Recent Lattice QCD calculations indeed verify that the probability of finding virtual quark-antiquark pairs in the QCD vacuum decreases systematically when quarks are added. In the thirty years since the discovery of the EMC effect, rapid progress has been made in measurements of the spin averaged EMC effect. On the other hand, there has been no experimental information on the spin dependence of the EMC effect. This spin dependent EMC effect emphasizes the quark polarization degrees of freedom within a nucleus, due to the spin-dependence of the coupling between the quarks and the strong field inside the nucleus. Since no measurements exist at present, it is likely that surprises await.

1.2 Physics motivation

1.2.1 Polarized EMC effect : Models

When viewed from the laboratory frame, the mechanism of deep inelastic scattering of virtual photon from a nuclear system is different for small and large Bjorken x. For a nuclear target, the virtual photon can scatter,

- incoherently from the constituents of the target nucleus or

- scatter coherently, in which more than one nucleon participates in the interaction.

It is well known that the latter is responsible for the nuclear effect known as "shadowing" seen at small x ($x < 0.05$). The underlying process that causes such effects can be

viewed as the virtual photon striking the nucleus first fluctuating into a quark-antiquark pair then potentially forming more complex configurations. These interactions occur if the distance $1/(2m_N x)$ during which the photon exists as a quark-antiquark-gluon fluctuation exceeds the size of the target. Between $0.05 \leq x \leq 0.2$ unpolarized structure function data show an enhancement. The exact mechanism responsible for this effect is not yet well understood. Nuclear effects for spin structure functions at small x have been extensively discussed for ^{3}He and ^{7}Li by V. Guzey and M. Strikman [1]. They calculate nuclear shadowing of g_1^A using an extension of the Gribov theory of nuclear shadowing in DIS [5]. The effects of enhancement in the region $0.05 \leq x \leq 0.2$ is modeled by requiring the conservation of the Bjorken sum rule. The results are shown in Fig. 2. They predict a 16% effect for nuclear shadowing and a 20-50% effect for enhancement of the ratio $g_{1A=7}^{n.s.}/g_{1N}^{n.s.}$ (where $n.s.$ stands for non-singlet).
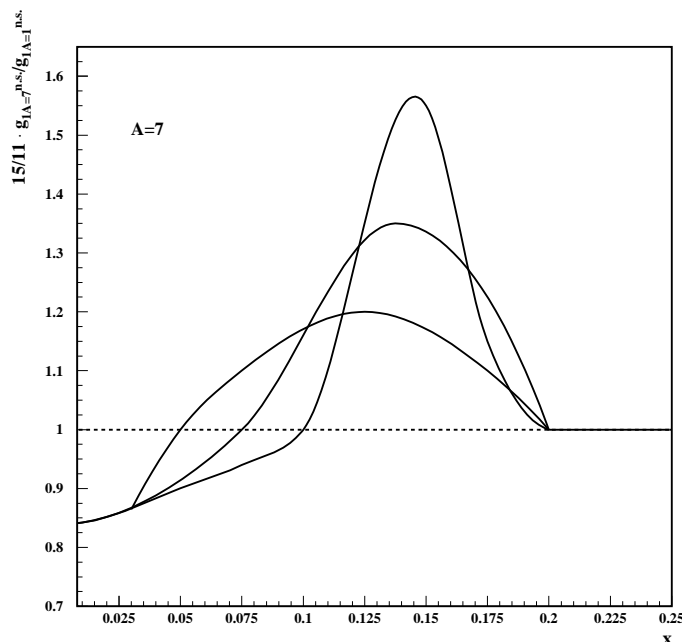

Figure 2: The figure shows the calculations of nuclear shadowing and modeling of the enhancement for the non-singlet combinations of spin structure functions. Three curves show three scenarios of the enhancement for ^{7}Li, which depends on the cross-over point between the regions of shadowing and enhancement.

Recently, intense theoretical effort has been invested in predicting the EMC effect in polarized structure functions in the moderate to high Bjorken x region ($\approx x > 0.2$). One such calculation by I. Cloet, W. Bentz and A. W. Thomas [2] predicts a significant effect, of order twice the size of the unpolarized EMC effect. To calculate the spin-dependent light cone quark distribution of a nucleus with mass number A and helicity H, they use the convolution formula,

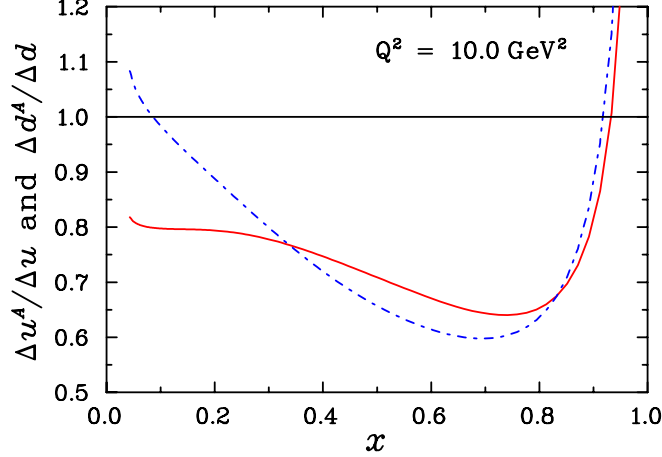$$\Delta f_{q/A}^{(H)}(x_A) = \int dy_A \int dx \, \delta(x_A - y_A \, x) \, \Delta f_{q/N}(x) \, \Delta f_{N/A}^{(H)}(y_A). \tag{1}$$

6

Figure 3: Ratio of the quark distributions in ^7Li to the corresponding free distributions, at a scale of $Q^2 = 10$ GeV^2. The solid line represents $\Delta u^A(x)/\Delta u(x)$ and the dot-dashed line $\Delta d^A(x)/\Delta d(x)$ [2].

In this formula, $\Delta f_{N/A}^{(H)}(y_A)$ is the light-cone momentum distribution of the nucleons in the nucleus and x_A is the Bjorken scaling variable for the nucleus. The term $\Delta f_{q/N}(x)$ is the spin-dependent quark light-cone momentum distribution in the bound nucleon. For the evaluation of this quark distribution, they describe the nucleon as a bound state of a quark-diquark in the Nambu-Jona-Lasinio (NJL) model. The distribution $\Delta f_{q/N}(x)$ is then obtained by straightforward Feynman diagram calculations. In this calculation the presence of the nuclear medium is taken into account through scalar and vector mean fields which act on the quarks in the nucleon.

- The in-medium effect of the scalar field is incorporated by replacing the free masses with the effective masses after the inclusion of Fermi motion. The Fermi motion of the nucleon is included by convoluting the spin-dependent quark distribution in the nucleon with a Fermi smearing function.

- The effect of the vector field is incorporated through a scale transformation of the spin-dependent light-cone quark distribution of the nucleus.

The effect on u and d quark distributions in nuclear matter at a scale of $Q^2 = 10$ GeV^2 is shown in Fig. 3. The ratio $\Delta q^A(x)/\Delta q(x)$ for $q = u, d$ is approximately the same in the large x region. Fig. 4 shows the EMC ratios F_{2N}^A/F_{2N} and g_{1p}^A/g_{1p} at nuclear matter densities. In the valence quark region, the spin-averaged model agrees very well with the data. For the spin-dependent case the model predicts even larger effects than the spin-averaged case. However these calculations are for nuclear matter. Calculations for light nuclei such as ^{15}N, ^{7}Li and ^{11}B have been published by the same authors in [3].

Another model by Jason Smith and Gerald Miller [4] emphasizes the importance of including the sea quarks. The main difference between the model by Cloet, Bentz and
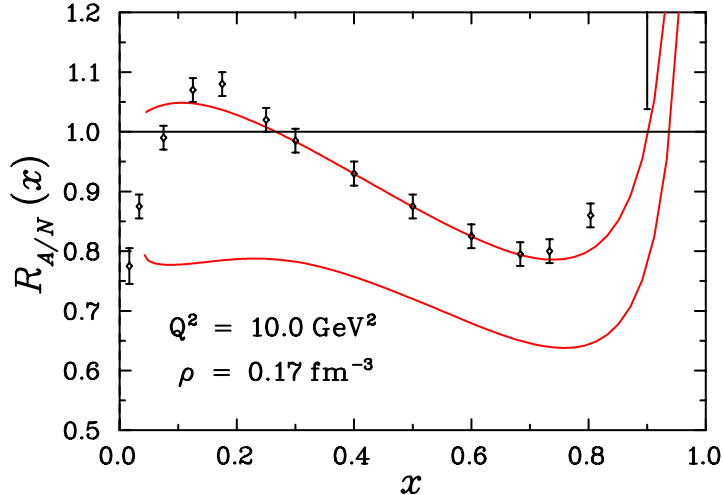
Figure 4: Ratios of the spin-independent and spin-dependent nuclear to nucleon structure functions at nuclear matter density [2]. The top curve is the ratio F_{2N}^A/F_{2N} for nuclear matter. Model predictions for the polarized EMC effect, g_{1p}^A/g_{1p}, is shown by the lower curve.

Thomas and that of Smith and Miller is that the latter includes sea quarks, while the former is essentially a valence quark picture. The main argument made by Smith and Miller is that any description of the EMC effect must be consistent with the constraints set by both deep inelastic scattering and Drell-Yan data. In the Drell-Yan process, quarks and antiquarks from hadron beams and nuclear targets annihilate each other and produce virtual photons that subsequently decay into lepton pairs. A great virtue of the process is that it can be used to examine the sea quark distribution of the nucleus. In this model the medium modifications in both valence and sea quark distributions are calculated within the chiral quark-soliton (CQS) model [8, 9, 10, 11, 12]. One of the drawbacks of the CQS model, in the form used in the calculations, is that it fails to recognize that quarks and gluons are never seen as free particles, or in other words, confinement. Despite that confinement is not implemented in this model, the calculations reproduce the trend of unpolarized (F_{2N}^A/F_{2N}) and Drell-Yan data [13] within the accuracy of current experiments. Fig. 5 shows the EMC ratio

$$
\begin{aligned}
R_1(x, Q^2) &= \frac{g_1^{(p|A)}(x, Q^2, k_F)}{A g_1^{(p)}(x, Q^2, k_F = 0)}, \\
g_1^{(p|A)}(x, Q^2, k_F) &= \int_x^A \frac{dy}{y} f(y) g_1^{(p)}(x/y, Q^2, k_F).
\end{aligned}
\tag{2}
$$

The heavy line is the full calculation for nuclear matter and the light line is if only valence quarks are included. The effects calculated at the valence quark level are similar to the effects predicted by [2]. The full calculation shows a large enhancement for $x < 0.3$ due to the sea quarks, suggesting a significant effect should be present in polarized Drell-Yan experiments compared to the unpolarized case.
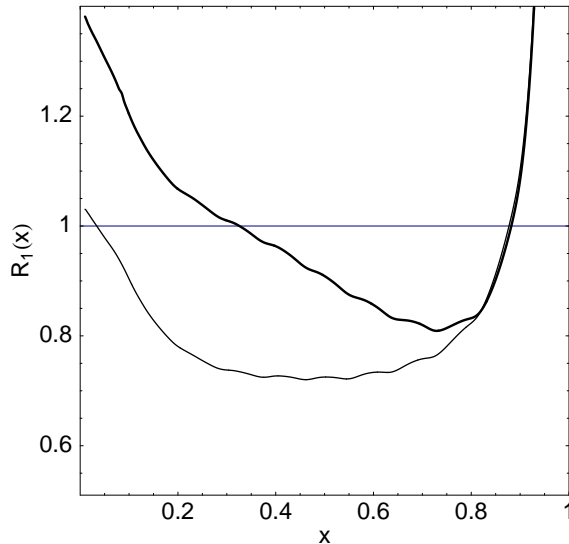
8

Figure 5: The ratio Eq. (2) at scale $Q^2 = 10$ GeV^2 for nuclear matter in the model of Smith and Miller [4]. The heavy line is the full calculation for nuclear matter, which includes sea quarks. The light line is the effect calculated using only valence quarks at the model scale.

1.2.2 Proposed experiment at Jlab

Although significant progress has been made in the theory for the polarized EMC effect, the ratio still remains unmeasured. We plan to make the first measurement of the polarized EMC ratio for the proton using a ^{7}Li target in the $0.1 < x < 0.7$. The full Q^2 and x coverage is given in Fig. 6. This kinematic region covers the DIS region as well as the resonance region. Our measurement of the polarized EMC effect will test the two theoretical predictions currently available. The two models differ significantly in the region $0.3 < x < 0.5$, particularly in the x dependence of the function, which is significant in that the proposed measurement will be able to determine the shape of the EMC ratio with higher precision than the absolute value of the ratio. Preference towards one prediction over the other would indicate the role sea quarks play in the medium modifications. Our pioneering measurement will help us understand the role played by both quarks and antiquarks in nuclei.

2 Overview of the experiment

For this experiment we will use the base 12 GeV equipment, plus the new EG12 target instrumentation, together with potential small modifications to accommodate the specific target material utilized. We affirm that the previously stated intentions of the collaboration to participate in and contribute to the construction of the base equipment and additional approved equipment is still in effect, and progress toward the fulfillment
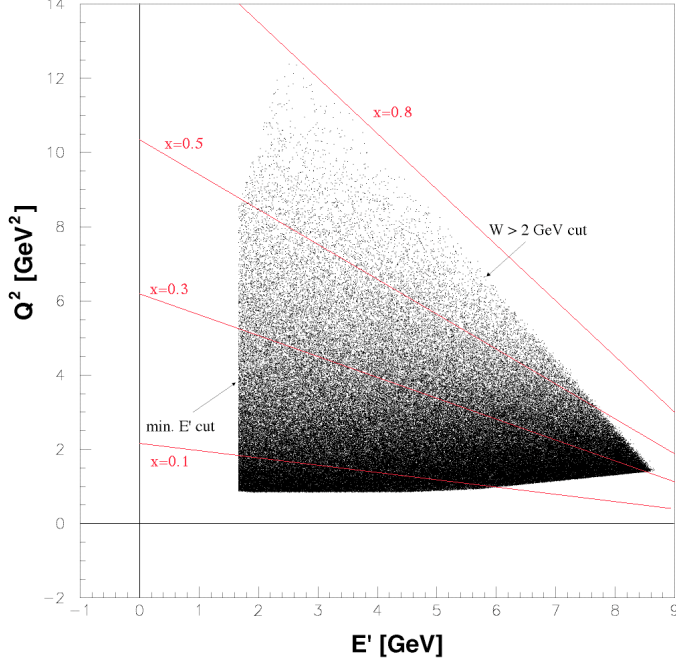
Figure 6: The plot shows the kinematic coverage of the intended measurement.

of those intentions has been visible in a number of places. One such example is a request for MRI funds that has been submitted to NSF to build the new polarized target: "MRI-Consortium for the Development and Construction of a Longitudinally Polarized Proton and Deuteron Target for CLAS12 at Jefferson Lab" (S. Bueltmann, S. Kuhn, D. Crabb, D. Day, Y. Prok, E. Brash).

2.1 Experimental setup and kinematics

We plan to cover the kinematic region shown in Fig. 6, for 11 GeV beam energy. This beam energy was selected to choose the maximum possible coverage for the DIS scattering. We plan to scatter longitudinally polarized electrons from polarized protons. The scattered electrons will be detected with CLAS12.

2.2 Target

We plan to use the same target setup as in the EG12 experiment. Thus, we can capitalize on the operational experience with this target during the EG12 run. It should be noted that the considerable expertise of the JLab polarized target group will also be significantly augmented by our collaboration on this experiment, many of whom have a high degree of experience with such targets. This same Since polarizing the nucleus results in a variety of spin combinations of the nucleons, an unambiguous extraction of $g_1^{p|A}$ can be done only for few special nuclei. ^{7}Li is a good example of one such nucleus and also a

10

realistic polarized target. We choose to polarize ^{7}Li using a ^{7}LiH target. Since we choose to use Dynamic Nuclear Polarization (DNP) to polarize the target, both the ^{7}Li and ^{1}H nuclei will be polarized. In principle, it is possible to reduce the proton polarization by saturating the proton's NMR transition, however this can be detrimental to the ^{7}Li polarization as well. This has to be further investigated. The ^{7}LiH beads will be immersed in a liquid He bath for cooling purposes and the target will be continuously polarized. Without any further developments to the present target system we expect to achieve a target polarization of 80%. However we need to do more research and development to optimize the target polarization. Studies of the optimization of the polarization of ^{7}LiH have not been as extensive as that for ^{6}LiD [14],[15], particularly at our conditions of 5 T and $\approx$ 1 K. Measurements at Saclay [16] showed that for irradiations of between 2-3 $\times$ 10^{17}electrons cm^{-2} at the appropriate irradiation temperature (180 - 190 K), polarizations of about 55% and 45% for proton and ^{7}Li respectively were obtainable in a dilution refrigerator and with a field of 2.5 T. Increasing the field to 5 T increased the polarizations to 70% and 50%. The only measurements of 5 T and 1 K that we are aware of were made at UVA with ^{7}LiH that was irradiated under less than optimal conditions, many years before. Proton polarizations of about 21% and ^{7}Li polarizations of 12% were achieved after about 3.5 hours of operation and were still increasing at a reasonable rate. The Abragam group measured about 94% polarization for ^7LiH[21] with a 6.5 Tesla magnetic field. Because they achieved such high polarization, for the purposes of this document we have assumed that we can reach 80% polarization in a practical setup and with our 5 T field, after some further R&D. It has been noted [14] that the lithium hydrides have very long polarizing times after the initial irradiation. However, when it is exposed to ionizing radiation in the polarizing cryostat, the polarizing time reduces by a factor of 5 to 6. The achievable polarization also increases by a relative 25%. Other techniques such as 'tempering' also improve the polarization performance of ^{7}LiH.

Optimization of the irradiation parameters can be investigated using the electron Linac at NIST and polarizing at UVA. Though the Equal Spin Temperature (EST) theory [17] is well established for the lithium hydrides, it will not be difficult to test and calibrate for the particular samples which will be used in the experiment.

The Hall B/EG1 polarized target insert consists of four cells that contain the target material. In addition to ^{7}LiH, we plan to fill the other three target cells with unpolarized ^{12}C, pure ^{7}Li and liquid He. The data taken with the ^{12}C, ^{7}Li and liquid He targets will be used to constrain the dilution factor of the ^{7}LiH, while pure ^{7}Li data will also be used to refine the unpolarized structure function model of F_1 for ^{7}Li.

3   Formalism

The inclusive doubly polarized electron-nucleon cross section for longitudinally polarized target and beam can be written as,

$$\frac{d\sigma}{d\Omega dE'} = \Gamma_T[\sigma_T + \epsilon\sigma_L + P_e P_t(\sqrt{1-\epsilon^2}A_1\sigma_T cos\psi + \sqrt{2\epsilon(1+\epsilon)}A_2\sigma_T sin\psi)], \quad (3)$$

where Γ_T is the transverse flux factor, A_1 and A_2 are the virtual photon asymmetries, ψ is the angle between the target spin and the virtual photon direction, σ_T and σ_L are the total absorption cross sections for transverse and longitudinal virtual photons and ϵ is the polarization parameter of the virtual photon.

The asymmetry $A_\parallel$ for longitudinally polarized beam and target is given by:

$$A_\parallel = \frac{\frac{d^2\sigma^{\uparrow\downarrow}}{d\Omega dE'} - \frac{d^2\sigma^{\uparrow\uparrow}}{d\Omega dE'}}{\frac{d^2\sigma^{\uparrow\downarrow}}{d\Omega dE'} + \frac{d^2\sigma^{\uparrow\uparrow}}{d\Omega dE'}} = D\left(A_1 + \eta A_2\right), \tag{4}$$

where $\frac{d\sigma^{\uparrow\downarrow}}{d\Omega dE'}(\frac{d\sigma^{\uparrow\uparrow}}{d\Omega dE'})$ is the differential cross section for the target spin antiparallel (parallel) to the beam helicity and D and η are

$$D = \frac{1 - \epsilon E'/E}{1 + \epsilon R}, \qquad \eta = \frac{\epsilon\sqrt{Q^2}/E}{1 - \epsilon E'/E}. \tag{5}$$

The spin structure function g_1 is related to the experimental asymmetry $A_\parallel$ by

$$g_1(x, Q^2) = \frac{\tau}{1 + \tau}[A_1 + \frac{1}{\sqrt{\tau}}A_2]F_1(x, Q^2), \tag{6}$$

where

$$\tau = \frac{\nu^2}{Q^2}, \tag{7}$$

$$\epsilon = \frac{1}{1 + 2tan^2\frac{\theta}{2}\left(1 + \frac{\nu^2}{Q^2}\right)}, \tag{8}$$

and

$$R = \frac{2\sigma^L_{1/2}}{\sigma^T_{1/2} + \sigma^T_{3/2}}. \tag{9}$$

The ratio R is related to the unpolarized structure functions F_1 and F_2 by the relation,

$$R = \frac{F_2}{2xF_1}\left(1 + \frac{4M^2x^2}{Q^2}\right) - 1. \tag{10}$$

4 Experimental method

4.1 Extraction of g_1 using asymmetries

The experimental asymmetry given in equation (4) is measured by observing scattering rates,

$$A_\parallel^{meas} = \frac{C_{back}}{P_bP_tF_{DF}}\left(\frac{n^+ - n^-}{n^+ + n^-}\right), \tag{11}$$

where $n^+(n^-)$ are the raw counting rates normalized to the accumulated beam charge for beam helicity parallel (antiparallel) to the target spin, P_t is the target polarization,

P_b the beam polarization, F_{DF} the target dilution factor and C_{back} is a correction due to the presence of electrons which are coming from pair symmetric processes and pions in the electron sample. In addition radiative effects also have to be taken into account. The raw asymmetry $A_{raw} = \frac{n^+ - n^-}{n^+ + n^-}$ includes both the free proton asymmetry and the asymmetry due to ^{7}Li,

$$A_{^7Li} = \frac{A_{raw}C_{back}}{P_bP_tF_{DF}} - CA_p. \tag{12}$$

CA_p is a correction to the measured asymmetry due to the presence of polarizable free protons in the target. How the constant C is determined will be discussed in 4.1.5.

The g_1 will be extracted from $A_{^7Li}$ (after radiative corrections) in the following way,

$$g_1^{^7Li} = \frac{\tau}{1+\tau}\left[\frac{A_{^7Li}}{D} + \left(\frac{1}{\sqrt{\tau}} - \eta\right)A_2^{^7Li}\right]F_1^{^7Li}. \tag{13}$$

4.1.1 Model for $A_2(x, Q^2)$

We are planning to model A_2 in a similar manner as was done in the EG1 experiment (E 91-023/E 93-009) in Hall B. There are several constraints we can impose on A_2. One such constraint is the "Soffer Bound" [18],

$$|A_2| < \sqrt{R(1+A_1)/2}. \tag{14}$$

This takes into account the fact that $\sigma_{LT} \leq \sqrt{\sigma_L \sigma_T^{1/2}}$. A_2 is directly proportional to the combination $g_T(x, Q^2) = g_1(x, Q^2) + g_2(x, Q^2)$,

$$g_T(x, Q^2) = \frac{\nu}{Q}F_1(x, Q^2)A_2(x, Q^2). \tag{15}$$

The leading-twist prediction for g_T, g_T^{WW}, is the Wandzura-Wilczek [19] form,

$$g_T^{WW}(x, Q^2) = \int_x^1 \frac{g_1(x, Q^2)}{y}dy. \tag{16}$$

In the DIS region g_T^{WW} can be can be extracted from an iterative procedure. g_2 is expected to be small in the DIS region, and in the low Q^2 and resonance region an additional higher twist contribution has to be taken into account. Since our measurements are mainly in the DIS region this is not expected to create a significant systematic error. Fig. 7 compares g_1^p with the contribution from the unmeasured part.

4.1.2 Beam and target polarization

Since the asymmetry for elastic scattering off protons is well known, the product of beam and target polarization can be extracted using data

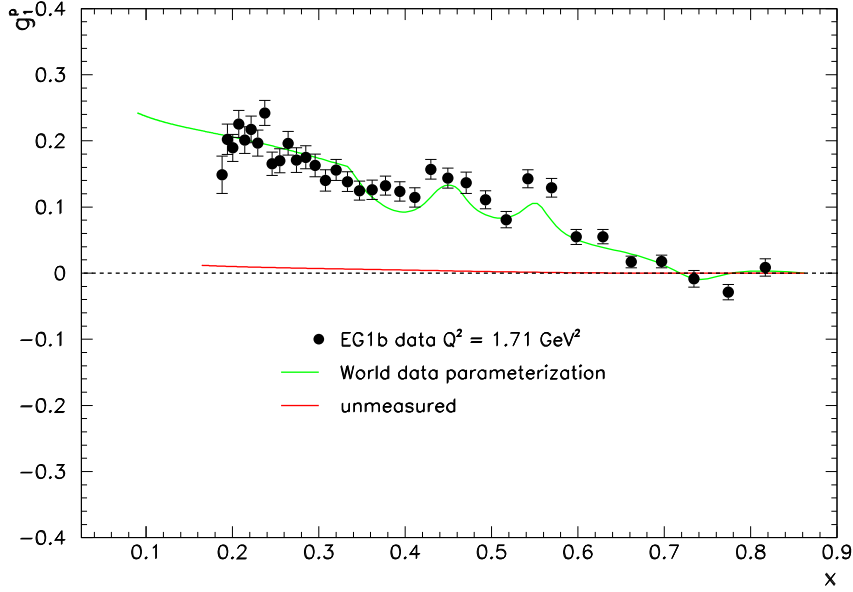$$P_bP_t = \frac{A_{el}^{meas}}{F_{DF}A_{el}^p}, \tag{17}$$

Figure 7: The figure compares the unmeasured contribution to g_1^p along with the EG1b results for g_1^p for $Q^2 = 1.71$ GeV^2.

where A^{meas} is the measured asymmetry in the elastic peak. The elastic asymmetry, A_{el}^p, for the proton can be calculated using [20],

$$A_{el}^p = \frac{\cos\theta^* \sqrt{1-\epsilon^2}A_1 + \sin\theta^*\sqrt{2\epsilon(1-\epsilon)}A_2}{1 + \epsilon\frac{Q^2}{\nu^2}\frac{G_E^2(Q^2)}{G_M^2(Q^2)}}, \tag{18}$$

where θ^* is the polar angle between the target spin direction and the direction of the virtual photon and the virtual photon asymmetries A_1 and A_2 for elastic scattering are given by,

$$A_1 = 1, \tag{19}$$

$$A_2 = \sqrt{\frac{Q^2}{\nu^2}} \left(\frac{G_E(Q^2)}{G_M(Q^2)} \right). \tag{20}$$

The quantities G_E and G_M are the electric and magnetic form factors of the proton. A_{el} depends only weakly on G_E^p/G_M^p, which introduces an error of $<1\%$ for $1 < Q^2 < 3$ GeV^2.

The product of beam and target polarization for the free proton can be extracted by measuring the elastic electron-proton coincidences. However the polarization of 7Li and H can be directly (and more precisely) measured by comparing the NMR signals, using two coils embedded in the target. We intend to measure the target polarization using

14

the latter method. We expect to achieve a 1% level accuracy for those measurements. Available data [21] on the ^{7}LiH target show that proton and ^{7}Li polarizations are in agreement with the Equal Spin Temperature (EST) theory [17] (Fig. 8). Direct measurements of ^{7}Li and ^{1}H collected at the Paul Scherrer Institute, which are not shown in the figure, are also consistent with the equal spin temperature theory [22].
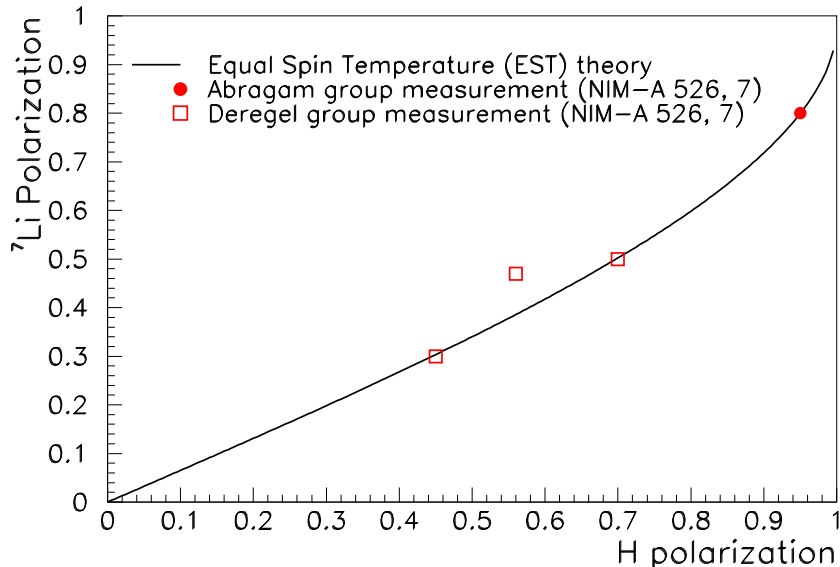

Figure 8: The polarization of ^{7}LiH versus that of proton. The curve is the theoretical prediction from the EST theory.

4.1.3 Dilution factor calculation

In this experiment we are interested only in scattering from the polarized ^{7}Li. Therefore to extract asymmetries it is necessary to correct for events from H. Since the ^{7}LiH beads will be immersed in a liquid He bath, it is important to remove the background contribution due to helium. To create an accurate background spectrum, helium as well as foils and target window materials also have to be taken into account. The dilution factor for ^{7}LiH is given by,

$$F_{DF} = \frac{N_{^7LiH} - N_{back}}{N_{^7LiH}},$$ (21)

where $N_{^7LiH}$ and N_{back} are the number of counts scattered from the ^{7}LiH target and the background materials. Since target material will consist of irregular shaped granules of varying sizes, the target thickness is not directly calculable. Instead the fraction of target material filling the target cup has to be determined. This quantity is called the

packing fraction. The dilution factor and the packing fraction will be determined using the data collected using all four targets, ^{7}LiH, ^{7}Li, ^{12}C and helium, as follows.

As a first step the normalized counts for targets, carbon (n_C), helium (n_{MT}) and LiH (n_{LiH}) can be written as sums of contributions from entrance and exit foils (F), helium (He), carbon (C) and deuterium,

$$n_{MT} = \left(\rho_F l_F \frac{\sigma_F}{\sigma_D} + \rho_{He} L \frac{\sigma_{He}}{\sigma_D} \right) F \sigma_D = \left(\rho_C l_C f \frac{\sigma_C}{\sigma_D} + \rho_{He} L \frac{\sigma_{He}}{\sigma_D} \right) F \sigma_D, \quad (22)$$

$$n_C = \left(\rho_C l_C (1 + f) \frac{\sigma_C}{\sigma_D} + \rho_{He} (L - l_C) \frac{\sigma_{He}}{\sigma_D} \right) F \sigma_D, \quad (23)$$

$$n_{LiH} = \left(\rho_C l_C f \frac{\sigma_C}{\sigma_D} + \rho_{He} (L - l_{LiH}) \frac{\sigma_{He}}{\sigma_D} + \rho_{LiH} l_{LiH} \frac{\sigma_{LiH}}{\sigma_D} \right) F \sigma_D, \quad (24)$$

where ρ is the density in moles per cm^3 and l the length of each component. The cross sections are in cm^2 per nucleus. The factor F contains all conversion factors and the acceptance and overall efficiency of CLAS12 at a given kinematic point and f is the contribution to the count rate from all foils combined, expressed as a fixed fraction of the contribution from ^{12}C in the carbon target. Using equations (22) and (23), normalized counts from the ^{12}C slab only, $\rho_C l_C \sigma_C = n'_{12C}$ and the counts per 1 cm length of liquid ^{4}He, $\rho_{He} \sigma_{He} = n'_{4He}$, can be obtained,

$$n'_{12C} = \frac{L}{L + f l_C} n_C - \frac{L - l_C}{L + f l_C} n_{MT}, \quad (25)$$

$$n'_{4He} = \frac{1 + f}{L + f l_C} n_{MT} - \frac{f}{L + f l_C} n_C. \quad (26)$$

Similarly, by writing the contribution to the count rate from all foils combined expressed as a fixed fraction of the contribution from ^{7}Li in the lithium target, f', normalized counts from the ^{7}Li slab only $\rho_{Li} l_{Li} \sigma_{Li} = n'_{7Li}$ can be obtained:

$$n_{MT} = \left(\rho_F l_F \frac{\sigma_F}{\sigma_D} + \rho_{He} L \frac{\sigma_{He}}{\sigma_D} \right) F \sigma_D = \left(\rho_{Li} l_{Li} f' \frac{\sigma_{Li}}{\sigma_D} + \rho_{He} L \frac{\sigma_{He}}{\sigma_D} \right) F \sigma_D, \quad (27)$$

$$n_{Li} = \left(\rho_{Li} l_{Li} f' \frac{\sigma_{Li}}{\sigma_D} + \rho_{He} (L - l_{Li}) \frac{\sigma_{He}}{\sigma_D} + \rho_{Li} l_{Li} \frac{\sigma_{Li}}{\sigma_D} \right) F \sigma_D, \quad (28)$$

$$n'_{7Li} = \frac{L}{L + f' l_{Li}} n_{Li} - \frac{L - l_{Li}}{L + f' l_{Li}} n_{MT}. \quad (29)$$

Equation (24) can also be written as,

$$n_{LiH} = \left(\left[\rho_{LiH} l_{LiH} \left(\frac{\sigma_{Li}}{\sigma_C} + \frac{\sigma_H}{\sigma_C} \right) + \rho_C l_C f \right] \frac{n'_{12C}}{\rho_C l_C} + (L - l_A) n'_{4He} \right) \quad (30)$$

$$= n_{MT} + l_{LiH} \left(\left[\frac{\rho_{LiH}}{\rho_C l_C} \left(\frac{\sigma_{Li}}{\sigma_C} + \frac{\sigma_H}{\sigma_C} \right) \right] n'_{12C} - n'_{4He} \right).$$

Then the target length l_{LiH} can be obtained by assuming,

$$\frac{\sigma_H}{\sigma_C} = 0.5 \left(1 - \frac{\sigma_n}{\sigma_D} \right), \quad (31)$$

16

$$l_{LiH} = (n_{LiH} - n_{MT}) \bigg/ \left(\left[\frac{\rho_A}{\rho_C l_C}\left(\frac{\sigma_{Li}}{\sigma_C} + 0.5\left(1 - \frac{\sigma_n}{\sigma_D}\right)\right)\right]n'_{12C} - n'_{4He}\right). \qquad (32)$$

Where the quantity,

$$\frac{\sigma_{Li}}{\sigma_C} = \frac{n'_{7Li}\rho_C l_C}{n'_{12C}\rho_{Li} l_{Li}}, \qquad (33)$$

and σ_n/σ_D can be determined by using the known unpolarized proton and neutron structure function data. The total background N_{back} is then given by,

$$N_{back} = \left(\left[\rho_{LiH} l_{LiH}\left(\frac{\sigma_H}{\sigma_C}\right) + \rho_C l_C f\right]\frac{n'_{12C}}{\rho_C l_C} + (L - l_A)n'_{4He}\right) \qquad (34)$$

$$= n_{MT} + l_{LiH}\left(\left[\frac{\rho_{LiH}}{\rho_C l_C}\left(\frac{\sigma_H}{\sigma_C}\right)\right]n'_{12C} - n'_{4He}\right).$$

4.1.4 Tensor polarization of the target

Using a nucleus with spin 3/2 can lead to some complications. In particular, in addition to the desired vector polarization, the Boltzmann population of the four substates leads to tensor polarization of rank 0, 1, 2 and 3. Since we are planning to polarize the target along the beam direction (z-axis), the cross section could depend on polarization tensors t_{00} (=1), t_{10} (= P_z), t_{20} and t_{30}. We plan to take data with both positive and negative target polarization along the z-axis. Therefore when combined, the contribution from most of the unwanted polarization tensors will cancel out in the numerator of the asymmetry A_{7LiH}. However the other tensors will be present in the denominator, but will make a very small correction versus the leading t_{00} term, which is the unpolarized cross section. To extract any non-trivial modifications of the structure function, we need to compare the results to a classical nuclear physics calculation. We are planning to work with theoretical specialists to calculate the proper polarized spectral function to estimate any such effect.

4.1.5 Correcting the asymmetry for the free proton

To extract the ^{7}Li asymmetry from the measured ^{7}LiH asymmetry a correction due to polarized H has to be made. The measured count rates n^+ and n^- for positive and negative incident helicity can be written as,

$$n^+ + n^- = \Phi\left(N_p\sigma_p + N_{7Li}\sigma_{7Li}\right), \qquad (35)$$

where,

> Φ includes the acceptance and the flux of the incident beam,
> N_p is the number density of protons,
> N_{7Li} is the number density of lithium,

and σ_i are the corresponding radiated cross sections. Similarly,

$$n^+ - n^- = P_b\Phi(N_p\sigma_p A_p P_p + N_{7Li}\sigma_{7Li}A_{7Li}P_{7Li}), \qquad (36)$$

where A_p and A_{7Li} are the corresponding radiated asymmetries and P_p, P_{7Li} are the corresponding polarizations of the materials given above. For simplicity we haven't included the other possible polarizable materials in the target. In practice those materials will be included and corrected accordingly. The measured asymmetry is then,

$$A_{raw} = \frac{n^+ - n^-}{n^+ + n^-} = P_b P_{7Li} f \left(A_{7Li} + \frac{N_p}{N_{7Li}} \frac{\sigma_p}{\sigma_{7Li}} \frac{P_p}{P_{7Li}} A_p \right), \tag{37}$$

where,

$$f = \frac{N_{7Li}\sigma_{7Li}}{N_{7Li}\sigma_{7Li} + N_p\sigma_p}, \tag{38}$$

which was described in section 4.1.3. The ^{7}Li asymmetry can then be extracted as follows,

$$A_{7Li} = \frac{A_{raw}}{P_b P_{7Li} f} - \frac{N_p}{N_{7Li}} \frac{\sigma_p}{\sigma_{7Li}} \frac{P_p}{P_{7Li}} A_p. \tag{39}$$

σ_{7Li} will be extracted from ^{7}Li data for each kinematic bin. Note that $N_p/N_{7Li} = 1$. The free proton radiated asymmetry A_p is known quite accurately and we intend to use similar methods to those which were employed in the experiments at SLAC and in the JLab EG1 measurements.

4.1.6 F_1 and $R = \sigma_L/\sigma_T$ for ^{7}Li

Available data suggest that nuclear effects seem to affect the structure functions F_1 and F_2 in a similar manner and to cancel in R. Fig. 9 shows the world's data for R_A/R_D for different nuclear targets as a function of Q^2 [23]. It is very clear from the figure that all data are consistent with unity in the Q^2 and x region of the intended measurement. Therefore we assume that $R_{7Li} = R_p$. For R_p we are planning to use the same model that was used in the analysis of EG1 data. In this model,

- The ratio R is calculated using the SLAC fit "R1998" [24], which is an update to the SLAC/Whitlow fit, "R1990" [25]. The data used in the fit cover the kinematic range of $0.005 \leq x \leq 0.86$ and $0.5 \leq Q^2 \leq 130$ GeV^2. The model includes three different parameterizations for R. The model uses the average of the three parameterizations. The uncertainty in R due to statistical fluctuations of the data is given by the error of the fit,

$$\delta R(x, Q^2) = 0.0078 - 0.013x + \frac{0.070 - 0.39x + 0.70x^2}{1.7 + Q^2}. \tag{40}$$

  The fit has a confidence level of 73% for all the data used in the fit.

- In the resonance region a fit to the recent Hall C data performed by Eric Christy is used.
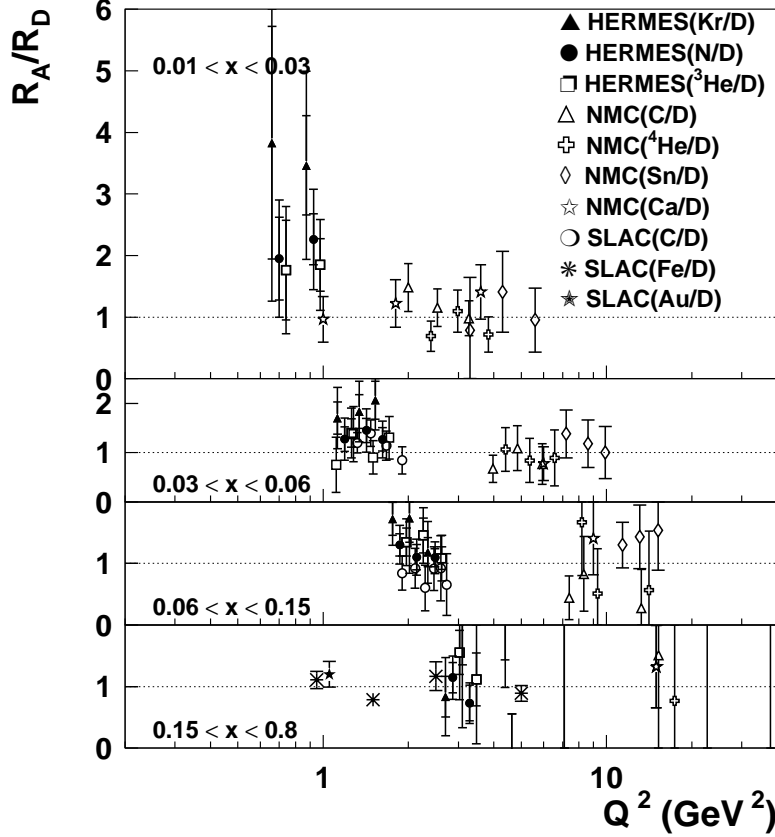
Figure 9: The ratio R_A/R_D for several nuclear targets with respect to deuterium as a function of Q^2 [23].

The resonance region and the DIS region are combined using a smooth interpolation. Since the proposed measurements are for $Q^2 > 0.7$ GeV^2 the low Q^2 resonance region, which is relatively unmeasured, is not a concern.

To extract g_1 we also need to know the unpolarized structure function F_1 of ^{7}Li. The data collected using the unpolarized pure ^{7}Li target will also be used to improve the unpolarized structure functions for ^{7}Li in addition to using that data, to determine the dilution factor of the target.

4.1.7 From $g_1^{^7\text{Li}}$ to $g_1^{p|^7\text{Li}}$

The determination of the $g_1^{p|^7Li}$ from a measurement on $g_1^{^7Li}$ relies on our understanding of the reaction mechanism of the virtual photon combined with the use of a realistic ^{7}Li wave function. The ^{7}Li nucleus has total angular momentum $J = 3/2$, negative parity and dipole moment $\mu = 3.26\mu_N$. In the single particle shell model ^{7}Li can be described as a combination of one unpaired proton and two paired neutrons in the $P_{3/2}$ state, and a closed $S_{1/2}$ shell (Fig. 10). In the shell model the ground-state wave function of ^{7}Li

19

with the z component $M_J = 3/2$ is given by [1],

$$\Psi_{Li-7}^{3/2} = \frac{3}{\sqrt{15}} \left[\Psi_p^{3/2} \Psi_n^{3/2} \Psi_n^{-3/2} \right] - \frac{2}{\sqrt{15}} \left[\Psi_p^{3/2} \Psi_n^{1/2} \Psi_n^{-1/2} \right] \tag{41}$$
$$- \frac{1}{\sqrt{15}} \left[\Psi_p^{1/2} \Psi_n^{3/2} \Psi_n^{-1/2} \right] + \frac{1}{\sqrt{15}} \left[\Psi_p^{-1/2} \Psi_n^{3/2} \Psi_n^{1/2} \right].$$

The wave function with $M_J = 1/2$ is given by,

$$\Psi_{Li-7}^{1/2} = \frac{1}{\sqrt{15}} \left[\Psi_p^{3/2} \Psi_n^{1/2} \Psi_n^{-3/2} \right] - \frac{2}{\sqrt{15}} \left[\Psi_p^{1/2} \Psi_n^{3/2} \Psi_n^{-3/2} \right] \tag{42}$$
$$- \frac{3}{\sqrt{15}} \left[\Psi_p^{1/2} \Psi_n^{1/2} \Psi_n^{-1/2} \right] + \frac{1}{\sqrt{15}} \left[\Psi_p^{-3/2} \Psi_n^{3/2} \Psi_n^{1/2} \right].$$

The $M_J = -1/2, -3/2$ wave functions can also be obtained in a similar way. Therefore according to the simple ground state shell model, the ^{7}Li nuclear polarization is due to a single proton 87% of the time.

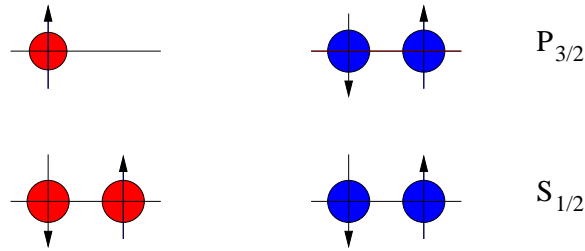Figure 10: The shell model description of ^{7}Li.

The possibility of using clusters instead of nucleons to describe the ^{7}Li nucleus is discussed in [26]. In this model ^{7}Li is considered as containing α particle and triton cluster. It can be viewed as a $S = 1/2$ triton orbiting in an $L = 1$ state about the α cluster as shown in Fig. 11. The four $M = \pm 3/2, \pm 1/2$ substates have equal probability. In the $+3/2$ sub state the triton and the ^{7}Li spins are given by[27],

$$\left| \pm 1, \pm \frac{1}{2}, \pm \frac{3}{2} \right\rangle,$$

where the notation is, $CG \left| m_L, m_S, M \right\rangle$ and CG is the Clebsch-Gordan coefficient of a given sub state. This approach gives the result that the total polarization in the ^{7}Li is 86%. More advanced Green's-function Monte Carlo (GFMC) calculations for the ^{7}Li nucleus have been performed in [28]. These calculations predict 89% proton polarization and -4% neutron polarization, which agree quite well with the cluster model calculations. The high degree of consistency between the proton polarization found in the cluster approach (86%) and the highly sophisticated GFMC approach (89%) demonstrates that the uncertainty in these measurements due to nuclear effects is very small.
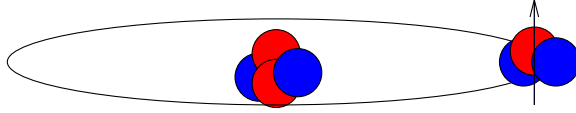
Figure 11: The cluster model description of ^{7}Li.

In closing this section, it is important to emphasize that the above shell model discussion is intended simply to illustrate the origin of the high polarization of the embedded proton; we **do not intend to use simple shell model estimates** to determine the degree of polarization alignment between the unpaired proton in ^7Li and the ^7Li nucleus overall. This crucial number, of approximately 89%, will be taken from the sophisticated Quantum Monte Carlo calculations such as the Green's Function Monte Carlo (GFMC). These approaches typically describes static properties of the nucleus to an accuracy of 1-2% for the ground state and lower excited states of nuclei with $A < 13$. These state-of-the-art calculations are very well known within the nuclear structure community, but may not be familiar to a broader circle of readers; they represent the culmination of a three decade sustained effort to derive nuclear properties rigorously from the NN interactions and known fundamental properties of the interactions. An illustration of the precision achieved in these approaches can be seen in Fig. 12, which shows the energies of the ground states and lower excited states of the A=6-8 nuclei. The very small discrepancies between the IL2 approach and the excited states which have measured experimental values are typically less than 100 keV. We recognize that this is a crucial aspect of the extraction of the EMC ratio from the precise experimental polarization measurement in the ^7Li system, and thus we will collaborate with the groups carrying out these calculations to do careful evaluations of the uncertainties for polarization observables, as well as exploring experimental cross-checks that can be performed.

5   Expected results

We are primarily interested in the deep inelastic scattering region because most model calculations are based on inelastic scattering. We are planning to propose a measurement of inclusive electron scattering from ^{7}Li. Scattered electrons will be measured in CLAS12. As mentioned previously the existing polarized target setup will be used. Data will be taken with high-energy beam, preferably 11 GeV, and with inbending torus current settings in CLAS12. Fig. 13 shows the projected errors for $R_{EMC} = g_1^{p|A}/g_1^p$ calculated from the 30 days of the EG12 inbending running scaled to 70 days of inbending data at 12 GeV. An additional scale factor was used to take into account the correct dilution factor of ^{7}Li, an 80% target polarization and a beam polarization of 80%. Fig. 13 shows the statistical uncertainties we believe we can achieve. The estimated systematic uncertainties depend partly on technical progress expected to be achieved by the time of running. The estimates for the systematic uncertainties on the absolute value of the EMC ratio currently range from 5-7%, based on the extensive experience gained from the
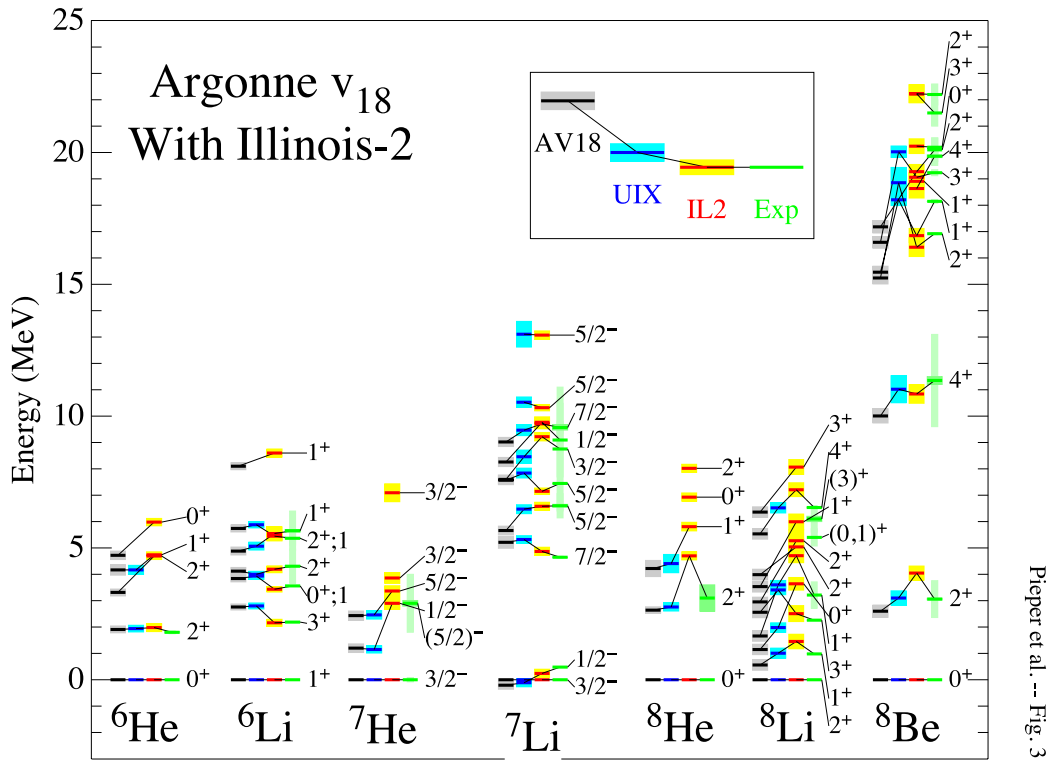
Figure 12: Green's Function Monte Carlo (GFCM) calculations for excited states in the A=6-8 region from [7]. This figure illustrates the precision achieved in these approaches. The energies of the ground states and lower excited states of the A=6-8 nuclei are plotted for several variants of Quantum Monte Carlo calculations, along with experimental data when it is available. The very small discrepancies between the IL2 approach and the excited states which have measured experimental values are typically less than 100 keV.
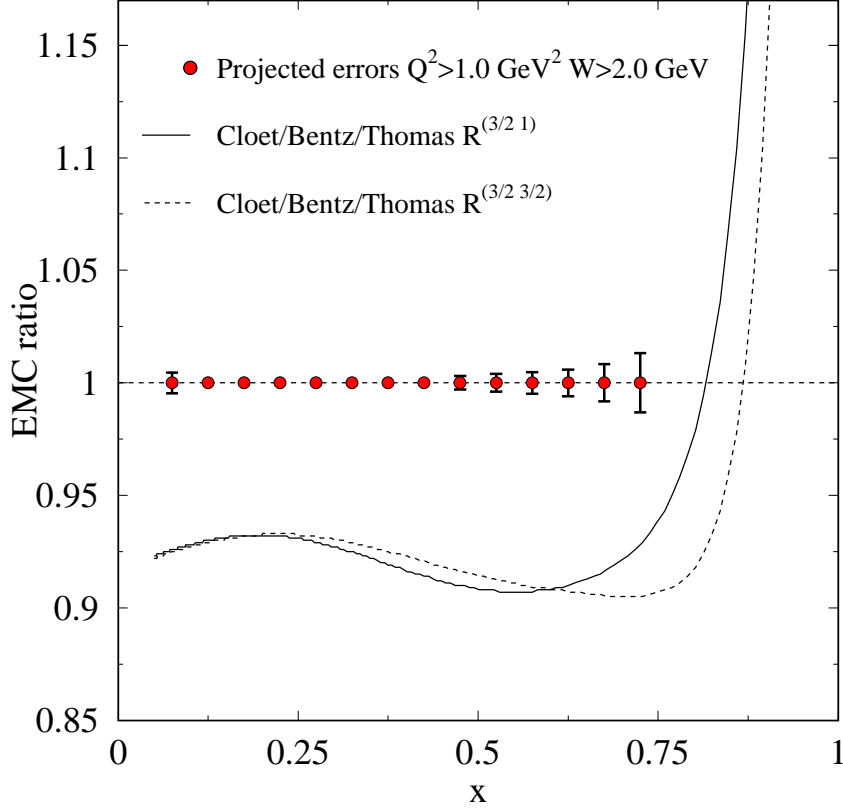
Figure 13: Projected statistical uncertainties for the ratio $g_1^{p|^7Li}/g_1^p$ as a function of x; see text for details. Also shown is (solid line and dashed line) the predictions by [3] specifically for ^7Li.

EG1 polarized target and the expected improvements in the new EG12 polarized target. It should be emphasized that the *shape* of the x dependence will be measured with a smaller uncertainty than is expected for the absolute value of the ratio. This precision is important in order to distinguish between current models for the polarized EMC ratio, which have a markedly different x dependence. In addition, we may be able to go to higher x by including the resonance region and invoking duality. It has been shown that duality works well for the unpolarized EMC effect [29]. The Fig. 14 shows the duality in the unpolarized EMC effect for three nuclear targets. The data clearly follow the DIS data. Duality is also proven to work well for polarized structure functions beyond the $\Delta(1232)$ resonance region. g_1^p is negative in the delta region, the EMC effect measures the ratio of g_1 of nuclear and nucleon data inducing a positive value. Therefore it is not unrealistic to expect similar effects as in the unpolarized case. The projected errors are compared to the theoretical calculations by [3] for ^7Li.
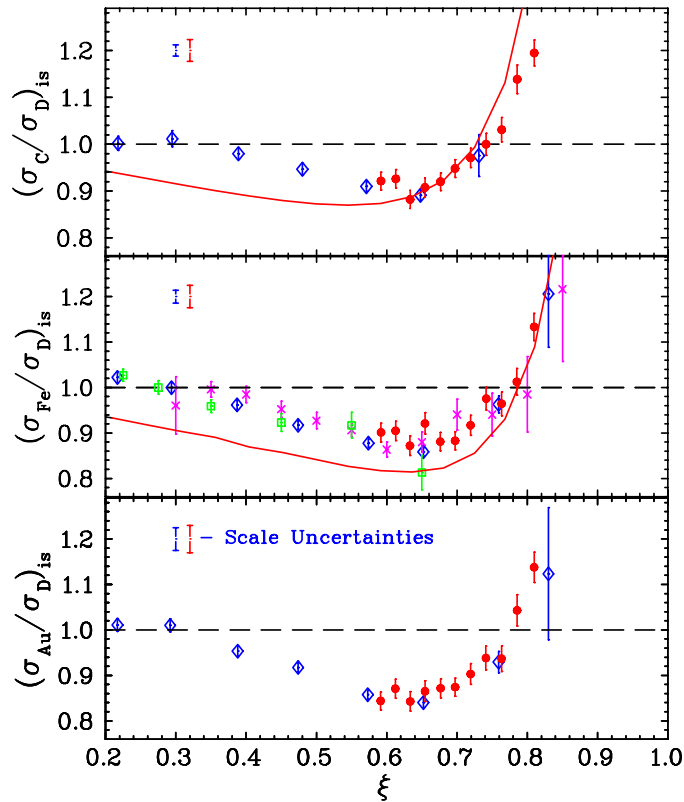
Figure 14: Comparison of nuclear to deuterium crossections for data collected in the resonance region and the DIS region. The solid circles are Jefferson lab data taken in the resonance region and the open markers are the data taken in the DIS region at SLAC and BCDMS. As it can be seen the resonance data are in agreement with DIS data.

6 Conclusion

We intend to perform the first measurement of the polarized EMC effect, $g_1^{p|^7Li}/g_1^p$, for $x > 0.1$. The absolute value of the polarized EMC ratio will be determined with good accuracy, and the shape of the x dependence of the ratio will be determined with high accuracy, which is important for distinguishing between current model calculations. The ratio will be determined from the fundamental quantity g_1^{7Li} through the use of high precision Quantum Monte Carlo calculations in light nuclei such as the Green's Function Monte Carlo. In order to optimize the polarized target technology for this measurement, we intend to do further research and development, investigating other technical options such as a pure ^7Li target, that will improve the systematic uncertainties significantly compared to the methods described herein.

References

[1] V. Guzey and M. Strikman, Phys. Rev. **C 61** 014002 (2000).

[2] I. Cloet, W. Bentz and A. W Thomas, Phys. Rev. Lett. **95**, 052302 (2005).

[3] I. Cloet, W. Bentz and A. W Thomas, Phys. Lett. B642 (2006) 210-217.

[4] J. R. Smith and G. A. Miller, Phys.Rev. **C 72** 022203 (2005).

[5] V. N. Gribov, Sov. J. Nucl. Phys. **9**, 369 (1969).

[6] I. Cloet, private communication.

[7] Steven C. Pieper, R. B. Wiringa, and J. Carlson, Phys. Rev. **C70** 054325, 2004.

[8] S. Kahana, G. Ripka and V. Soni, Nucl. Phys. A **415**, 351 (1984).

[9] M. C. Birse and M. K. Banerjee, Phys. Lett. B **136**, 284 (1984).

[10] D. Diakonov and V. Y. Petrov, in "At the Frontier of Particle Physics, Vol. 1" M. Shifman (ed.), World Scientific, Singapore, pp. 359-415 (2001).

[11] C. V. Christov *et al.*, Prog. Part. Nucl. Phys. **37**, 91 (1996).

[12] R. Alkofer, H. Reinhardt and H. Weigel, Phys. Rept. **265**, 139 (1996)

[13] J. R. Smith and G. A. Miller, Phys. Rev. C **70**, 065205 (2004)

[14] S. Goertz et al., Nucl. Instr. and Meth. in Phys. Res., A356, 20 (1995)

[15] S. Bültmann et al., Nucl. Instr. and Meth. in Phys. Res., A425, 23 (1999)

[16] P. Chaumette et al., High Energy Spin Physics Symposium, Minneapolis, 1988, AIP Conf. Proc.,187 Vol. II, 1275 (1989).

[17] D. G. Crabb and W. Meyer, Ann. Rev. Nuc. Part. Sci., **C 47**, 67 (1997).

[18] J. Soffer, O. V. Teryaev, hep-ph/0005132.

[19] S. Wandzura and F. Wilczek, Phys. Lett. **B 72**, 195 (1977).

[20] T. W. Donnelly and A. S. Raskin, Annals of Phys. **191**, 78 (1989).

[21] J. Ball, Nucl. Inst. and Meth. **A 526**, 7 (2004).

[22] B. A. Raue, Phys. Rev. **C 53**, 1005 (1996).

[23] HERMES Collaboration, hep-ex/0210068 (2002).

[24] K. Abe *et al.*, Phys. Lett. B **452**, 194 (1999).

[25] L. W. Whitlow *et al.*, Phys. Lett. B **250**, 193 (1990).

[26] H. Walliser and T. Flieshhbach, Phys. Rev. **C 31**, 2242 (1985).

[27] O. A. Rondon Phys. Rev. C **60**, 035201 (1999)

[28] B. S. Pudliner *et al.*, Phys. Rev. **C 4**, 1720 (1997).

[29] J. Arrington, R. Ent, C.E. Keppel,J. Mammei and I. Niculescu, nucl-ex/0307012.